Targeting Semaphorin 7a signaling in preclinical models of estrogen receptor-positive breast cancer

ABSTRACT

Estrogen receptor-positive (ER+) breast cancer (BC) comprises over 70% of breast cancers and is the leading cause of BC-related deaths in women worldwide. Despite available therapies against ER+ BC, recurrence occurs in many patients due to therapeutic resistance. Semaphorin 7a (SEMA7A) is a biomarker associated with poor prognosis and endocrine therapy resistance for BC patients. Survival analyses of ER+ BC patients on endocrine therapy confirm early recurrence in patients with SEMA7A+ tumors. Thus, we aim to establish novel treatment strategies to improve outcomes for patients with ER+ SEMA7A+ BC. In this paper we investigate the mechanisms by which SEMA7A promotes resistance to endocrine therapy and its potential as a therapeutic target for ER+ BC. Our studies suggest that SEMA7A binds to integrins β1 and β4 (ITGB1, ITGB4) and activates AKT cell survival signaling via its RGD domain. Using a syngeneic ER+ model, TC11 tumors in FVB/N mice were treated with PI3K inhibitors (20mg/kg alpelisib; 10mg/kg GCT-007), alone or in combination with tamoxifen (0.5 mg/100uL peanut oil). TC11 tumors were also treated with a combination of an anti-SEMA7A antibody (SmAb H1) (100-250mg/kg) and fulvestrant (83mg/kg), compared to single agents. In vivo studies were validated in a second syngeneic ER+ model; SSM2 cells and 129SV-E mice. Our results demonstrate that direct inhibition of SEMA7A via SmAb H1 significantly reduces tumor growth of SEMA7A+ tumors, and the combination with fulvestrant may be even more effective. Our studies suggest that patients with ER+SEMA7A+ tumors should be candidates for PI3K-targeted therapies or anti-SEMA7A-based therapy.

INTRODUCTION

The most prevalent type of breast cancer (BC) is estrogen receptor-positive (ER+), accounting for 70% of all BC diagnoses (1,2). The standard treatment for women with ER+ BC typically involves endocrine therapy, such as the selective ER degrader, fulvestrant, or the selective ER modulator, tamoxifen (2,3). While endocrine therapy can be effective, eventually, 22-52% of patients with ER+ BC will experience disease recurrence, depending on lymph node involvement (2,3). Thus, there is an urgent need to improve treatments for patients with ER+ BC. We and others have identified that Semaphorin 7a (SEMA7A), a neuro-endocrine signaling protein (4), is dysregulated in various diseases and cancer types, resulting in poor prognosis (5-13). While numerous studies have investigated the role of SEMA7A in triple-negative breast cancer (TNBC), which lack expression of ER (ER-), progesterone receptor (PR-), and amplification of HER2 (HER2-) (14-19), to the best of our knowledge only our 2021 published studies have analyzed the importance of SEMA7A expression in ER+ BC (2). In this study, we observed that *SEMA7A* mRNA expression is elevated in 67% of luminal breast cancer cell lines, compared to 50% and 36% in basal A and basal B, respectively (2). In its immune-related and other roles, SEMA7A is known to bind to two receptors: Plexin C1 and Integrin β1 (ITGB1) (20), and in models of TNBC, we have shown that the pro-tumor roles for SEMA7A are dependent on ITGB1 and Integrin α6 (14,16). Known downstream targets of integrins are those involved in cell adhesion and cell survival, including the PI3K/AKT pathway. In support of a role for SEMA7A- and integrin-mediated activation of the PI3K pathway, studies in TNBC show activation of this pro-survival pathway (15). We have also shown that ER+SEMA7A+ tumors are sensitive to a non-selective PI3K inhibitor (LY294002), which is not utilized clinically (2,21). However, in the context of ER+ BC, the integrin receptors that SEMA7A binds to remain unknown. Previous studies have also demonstrated mechanisms of therapy resistance activated in ER+ SEMA7A+ tumors that drive reduced sensitivity to the endocrine therapy fulvestrant, including downregulation of ER, activation of pro-survival signaling through Bcl-2, and regulation of markers of drug-resistant stem cells (CD44+/CD24-) (2); the contribution of PI3K/AKT to these phenotypes is still unknown.

Constitutively active PI3K signaling can also lead to multidrug resistance, including fulvestrant resistance (22-24). We therefore sought to investigate the hypothesis that more specific PI3K inhibitors could be effective for ER+SEMA7A+BC. In our results presented herein, we show that breast cancer progression is increased in women with ER+SEMA7A+BC, resulting in poor prognosis and highlighting the need to identify additional treatment options. Mechanistically, we show for the first time that SEMA7A binds to an additional integrin, β4

(ITGB4), as well as ITGB1 in ER+ breast cancer cells and activates PI3K signaling as well as other phospho-signaling pathways related to cell survival in an integrin-dependent manner.

Integrins can also activate AKT directly through Integrin-linked kinase (ILK) phosphorylation of AKT at serine 473 (25). We have previously published that inhibitors of PI3K, ILK, and/or integrins can reduce SEMA7A-mediated activation of pAKT (26), but integrin and ILK inhibitors are not clinically available, so we studied the effect of PI3K inhibitors in SEMA7A+ tumors.

We also show partial reversal of endocrine therapy resistance in ER+SEMA7A+ models of breast cancer by PI3K inhibition. Finally, we test a novel anti-SEMA7A monoclonal antibody for specifically reducing tumor growth in mice harboring SEMA7A+ tumors, as a single agent and combined with fulvestrant. Collectively, our results support targeting of SEMA7A, both directly and indirectly through PI3K inhibition, as novel therapeutic strategies to improve patient outcomes in ER+SEMA7A+BC.

MATERIALS & METHODS

Cell Culture:
MCF7 cells were obtained from K. Horwitz (University of Colorado Anschutz Medical Campus). ZR75-1 cells were obtained from the University of Colorado Cancer Center Cell Technologies Shared Resource (CTSR). TC11 cells were obtained from L. Schuler (University of Wisconsin School of Veterinary Medicine). SSM2 cells were obtained from A. Borowsky (University of California Davis). Cell lines were validated by fingerprinting analysis at the University of Colorado Anschutz/Barbara Davis Center Molecular Biology Core. Cells were routinely tested for mycoplasma contamination throughout the studies described herein with Lonza MycLonza MycoAlert PLUS (Walkersville, MD); last tested 3-24-2025. Cells were cultured at 37°C and 5% CO2. MCF7 were grown in MEM with 5% heat-inactivated fetal bovine serum (FBS; Peak Serum PS-FB3, Colorado USA) and 1% penicillin/streptomycin (P/S; ThermoFisher Scientific). TC11 and ZR75-1 were grown in RMPI 1640 with 10% heat-inactivated FBS and 1% P/S. SSM2 were grown in DMEM/F12 and supplemented with 10% FBS, 1% L-glutamine, 1% P/S. 50 µM 2-mercaptoethanol, 0.3 µM hydrocortisone, 5 µg/ml insulin and 10 ng/ml transferrin. Experiments were performed with cells below passage 30. For exogenous SEMA7A treatments, recombinant SEMA7A (rSEMA7A) was purified from SEMA7A-Fc expressing MDA-MB-231 cells in collaboration with the University of Colorado Cancer Center CTSR (14,27).

Transductions:
MCF7-SEMA7A Overexpressing (OE) and MCF7-control (EV) cell populations were generated by lentiviral transductions with pLX304-Blast-V5 vectors; CMV-driven, V5-tagged full-length Semaphorin 7a cDNA (666 aa) or empty vector, respectively, and selected for using blasticidin at 5 µg/mL (Dana Farber Cancer Institute & CU Anschutz Functional Genomics Core). TC11-control and TC11-SEMA7A knockdown cell lines were generated via lentiviral transduction with pLKO-shNonTargeting-puro, and pLKO-shSEMA7A-038 (KD#1) and pLKO-shSEMA7A-040 (KD#2), respectively, and selected for using puromycin at 2 µg/mL. SEMA7A expression was validated via western blot analysis for all transduced cell lines.

Cell Viability Assays:
Cells were plated in a 96-well (1,000 cells/well), 24-well (100,000 cells/well), 12-well (200,000 cells/well) or 6-well (500,000 cells/well) plate in triplicate and allowed to adhere at 37°C for 24 hours. After 24 hours, the cells were treated with vehicle or drug as follows: Fulvestrant and 4-hydroxytamoxifen were purchased from Millipore Sigma (Cat#129453-61-8 and Cat#68392-35-8, St. Louis, MO). For *in vitro* assays, fulvestrant and 4-hydroxytamoxifen treatments were at a final concentration of 8 nM and 5 µM in DMSO, respectively. Alpelisib (BYL719) was purchased from SelleckChem (Cat# S2814) and used at 0.5-1 µM in DMSO, as determined by our dose response and the literature (28). GCT-007 was obtained via collaboration with Global Cancer Technology (San Diego, CA) and used at 0.1-0.5 µM in DMSO as determined by our dose response. Anti-Semaphorin 7a monoclonal antibody; clone H1 (SmAb H1) was obtained from the University of Colorado

Cancer Center CTSR. SmAb H1 or Mouse IgG1 (Bio X Cell; Cat# BP0083) was used at 1 μM in PBS as determined by our dose response and the literature (26,29,30). Percent confluence was determined via formalin fixation and 0.1% crystal violet staining and analyzed via ImageJ analysis. Data are normalized to control condition for each treatment. Experiments were performed in biological and technical triplicates and statistics were measured via repeated-measures two-way ANOVA with multiple comparisons.

Drug Titration Studies:
5,000 SEMA7A overexpressing or empty vector control MCF7 cells, OR 10,000 TC11 shCtrl or shSEMA7A cells, were seeded per well in a 96-well plate and allowed to adhere overnight. Vehicle or increasing concentrations of drug were added. Growth was assessed using 0.1% crystal violet staining after 24 hours of treatment. To calculate IC50 values, cell viability data for a range of concentrations (minimum 6-points data curve) for each drug was plotted as a dose-response curve in GraphPad Prism and analyzed using nonlinear regression three-parameters curve fit model of log(inhibitor) vs. response. Experiments were performed in triplicate and two-tailed, unpaired t-test was performed on each IC50 value in triplicate experminets.

Co-immunoprecipitation:
Pierce Classic Magnetic IP/Co-IP Kit (ThermoFisher; Cat# 88804) and User Guide/CoIP Protocol (Pierce Biotechnologies) was used to perform all CoIP experiments. Cells were cultured normally to optimal confluence in T75 flasks. For RGDS experiments, RGDS peptide (Tocris Bioscience; Cat#3498, 50uM in milliQ H_2O) or control (milliQ H_2O) was added to culture media for 1 hour prior to making cell lysates. Lysates were made using IP lysis/wash buffer and incubated on ice for 15 min followed by centrifugation. Protein concentration of lysates was quantified using Qubit Protein Broad Range Assay Kit (ThermoFisher; Cat# A50668). Per sample, 1.0 mg of lysate was pre-incubated with 30 uL IP antibody: mouse IgG or SEMA7A (Santa Cruz; Sc-374432) and rocked overnight at 4°C. Per sample, 25μl of Pierce Protein A/G magnetic beads were washed and incubated with the antibody-lysate solution and rocked for 1 hour at room temperature. Using a magnet, supernatant was removed, and the beads were washed with lysis buffer three times. Beads were then eluted with Pierce Elution Buffer, and 10uL (pH) Neutralization Buffer was added per sample. Non-reducing Lane Marker Sample Buffer (5X, Pierce) was used as loading buffer for immunoblots following CoIP elution.

Immunoblotting:
Protein extracts were prepared from cell lines by lysing cells in RIPA with EDTA (Thermo Fisher; Cat# J61529.AP) containing PhosSTOP phosphatase inhibitor (Roche; Cat# 4906837001), and complete protease inhibitor (Roche; Cat# 11697498001). Protein concentration of lysates was determined using Qubit Broad Range Protein Assay Kit (ThermoFisher; Cat# A50668). 30μg of total protein in Laemmli protein sample buffer was heated for 10 minutes. Lysates were run on SDS-Page gels and transferred onto methanol-activated PVDF membranes using the Trans-Blot Turbo Transfer System (Bio-Rad). Membranes were blocked with 5% bovine serum albumin and probed with the following primary antibodies according to manufacturer recommendation: SEMA7A (Santa Cruz; Cat#Sc-374432), pAKT S473 (Cell Signaling; Cat# 4060), total AKT (Cell Signaling; Cat#2920), ITGB4 (Cell Signaling; Cat#14803), ITGB1 (Cell Signaling; Cat#34971), ERα (AbCam; Cat#16660), α-tubulin (Cell Signaling; Cat +#9099S) and GAPDH (Biolegend; Cat# 607902). Membranes were washed with 1X Tris-buffered saline with Tween 20, incubated with a goat anti-rabbit HRP secondary antibody (Abcam; Cat# 6721), and developed with enhanced luminescence detection system (Thermo Fisher; Cat# 32106) on the Licor Odyssey. Densitometric O.D. values of three biological replicates were obtained using ImageJ(31) and normalized to the loading control GAPDH or α-tubulin, and normalized to the first sample.

Animal Experiments:
Power calculations based on pilot studies were utilized to determine the number of animals per group. Tumors were measured using digital calipers every 2–3 days with the observer blinded to treatment group, and tumor volume was calculated as (L × W × W × 0.5). Tumors were harvested at designated study endpoints (Maximum tumor volume = $1000mm^3$). Mammary glands with intact tumor, axial lymph nodes and lungs were harvested, formalin fixed, and paraffin embedded for immunohistochemical analysis. All animal studies were performed

under the approval of the UC Anschutz Medical Campus Institutional Animal Care and Use Committee. Beeswax estrogen (E2) and sham pellets were generated and administered based on previous literature (32). Beeswax estrogen (E2) and sham pellets were generated and administered based on previous literature (32). For the study that combined fulvestrant and rSmAb H1-P, tumors were harvested and detached from the mammary gland; photographs were taken next to ruler and scaled to 1cm scale bar.

MCF7 Model: MCF7 is a well-known human ER+ cell line used to study breast cancer, thus it was an appropriate model to initiate our studies. 2,500,000 SEMA7A overexpressing or control MCF7 cells were injected into the #4 mammary fat pads of 6–8-week-old female NCG mice (Cat# CRL572, Charles River, Wilmington, MA). For drug treatment studies, fulvestrant dosing began when average tumor volume reached ~100mm^3. At day 37, animals were randomized to treatment into size-matched groups to receive either vehicle or PI3K inhibitor (alpelisib or GCT-007) daily.

TC11 Model: TC11 is a syngeneic ER+ murine model which we chose to use because it provides the context of an intact immune system, and there are very limited other ER+ mouse models. TC11 also expresses endogenous SEMA7A, making it a relevant model for our research. 200,000 TC11 cells (wild type, shCtrl or shSEMA7A #2) were injected into the bilateral #4 mammary fat pads of 6–8-week-old female FVB/N mice (FVB/NCrl, Cat# CRL207, Charles River, Wilmington, MA). Mice were randomized to treatment into size-matched groups at average tumor volume ~50-100mm^3. For the estrogen/sham pilot study, mice were randomized to groups receiving E2 or sham pellets two days prior to tumor injections.

SSM2 Model: SSM2 is another syngeneic ER+ murine model which we chose to use because it provides the context of an intact immune system, and there are very limited other ER+ mouse models. SSM2 also expresses endogenous SEMA7A, making it a relevant model for our research. 1,000,000 SSM2 tumor cells were injected into the #4 mammary fat pads of 6–8-week-old female 129 Sv-E mice (129 Sv-E, Cat# CRL287, Charles River, Wilmington, MA). Mice were randomized to treatment into size-matched groups at average tumor volume ~50mm^3.

Treatments: Fulvestrant was administered as follows: 2.5 mg in 90% sesame oil and 10% ethanol, injected subcutaneously every 5 days. This dose is equivalent to approximately 83 mg/kg per mouse. Using the FDA Dosing Guidance for Industry: Conversion of Animal Doses to Human Equivalent Doses, equivalent to 6.7mg/kg in humans (2). Tamoxifen was given using the following dosing regimen: 0.5 mg/100uL peanut oil per mouse, via intraperitoneal (IP) injection every 3rd day (33). Alpelisib was dissolved in 1% Carboxymethyl cellulose solution + 0.5% Tween 80 and administered via oral gavage at 20 mg/kg daily. GCT-007 was dissolved in 55% 1M NaCl, 30% PEG-400, 7.5% Solutol-HS + 7.5% N-Methyl-2-pyrrolidone and administered via oral gavage at 10 mg/kg daily. SmAb H1/rSmAb H1 or Mouse IgG1 (Bio X Cell; Cat# BP0083) was given in sterile PBS at 100-250 µg per 100µL PBS every other day via IP injection (29,30).

Immunohistochemistry:

Tissue collected from the *in vivo* study endpoints as described above, was formalin-fixed and paraffin-embedded. Tissue was stained with Hematoxylin and Eosin. Four-µm sections were pretreated with 1X Dako Target Retrieval System. Slides were prepared in a Dako Autostainer with primary antibody (ITGB4: Cell Signaling Cat#14803, SEMA7A AbCam Cat # ab255602, 9EG7/CD29: BD Pharmingen rat-anti-mouse CD29 clone 9EG7 Cat# 550531), followed by EnVision+ HRP Rabbit Agilent Technologies cat# K4003 antibody for 30 mins. For 9EG7 staining, rat-on-mouse HRP polymer detection kit (Biocare cat# RT517H) was used for secondary. The tissue was incubated with chromogen 3,3'diaminobenzidine (Vector Labs catalog #SK-4105) for 10 minutes, and then the tissue was counter-stained with hematoxylin for 1 minute (Vector Labs catalog #H-3401-500). Stained images were acquired using an Olympus Fluorescent Microscope IX83. Quantification was performed using Cell Sense Analysis.

ELISA:

ELISA Buffer Kit (Thermo Cat #CNB0011) was used to perform an indirect ELISA where the plate was coated with SEMA7A protein and probed with serial dilution concentrations of rSmAb H1-P to determine binding specificity. A 96-well plate was pre-coated with 5ug/well of purified SEMA7A (50ug/mL) protein in Coating Buffer A and incubated at 4 degrees overnight. Plate was washed with 1X wash buffer and then probed with primary antibody (rSmAb H1-P) at serial dilution concentrations, from 20 to 0 ug/mL, and incubated at 4 degrees overnight. Plate was washed with 1X wash buffer three times and then probed with secondary antibody (Goat anti-mouse IgG-HRP; Abcam Cat#ab97040) for 30 minutes at room temperature. Plate was washed three times with 1X wash buffer and absorbance at 425nm was read on plate reader.

Data Mining Analysis:

Kaplan Meir Plotter(34) was used to assess overall survival (OS), distant metastasis-free survival (DMFS), and post-progression survival (PPS) data for BC patients in the ER+ dataset, and patients in the ER+ dataset who received endocrine therapy (tamoxifen or fulvestrant). SEMA7A was queried and stratified into high and low-expression groups using the auto-select best cutoff level function. The generated data, plots, hazard ratio (HR), and LogRank P value were downloaded from KMplotter.com. TCGA Human Data Analysis: We analyzed The Cancer Genome Atlas (TCGA) Breast Cancer study for the mRNA expression of *SEMA7A, ITGB1, and ITGB4* collected from patient samples processed by RNAseq – IlluminaHiSeq. Gene expression analysis was performed using the Xena Functional Genomics Explorer(35). The log2(norm_count+1) value for mRNA expression was used to graph correlations between SEMA7A and the other genes in the TCGA Breast Cancer dataset. Each data was analyzed using Pearson's correlation (rho) and p-values are indicated on each plot.

BioSpa Assay:

500 MCF7 cells per well were plated in 96 well plates and incubated overnight to allow for adherence. Cells were then treated with 1μM IgG1 or 1μM SmAb H1 and immediately placed in a BioSpa Live Cell Imager (Agilent) for 4 days, with images of each well being taken every 4 h, at ×10 magnification. The cell count of each well was measured via brightfield count in the BioSpa Software.

Reverse Phase Protein Array (RPPA):

For cell lysates: MCF7 Empty Vector control or SEMA7A Overexpressing cells were cultured, each in quadruplicate, in a 10cm dish for 72 h. After washing cells with PBS, lysates were generated using RPPA Lysis Buffer (Baylor College of Medicine Antibody-Based Proteomics Core) and frozen at -20°C. For tumors: tumors were harvested and flash-frozen in liquid nitrogen at necropsy and stored at -80°C. Lysates/tumors were shipped on dry ice to the Baylor College of Medicine (BCM) Antibody-Based Proteomics Core (Houston, TX). Subsequent RPPA was performed by the core facility as outlined here (https://www.bcm.edu/academic-centers/dan-l-duncan-comprehensive-cancer-center/research/cancer-center-shared-resources/antibody-based-proteomics/protocols-workflow) (36). Normalized fold change for each antibody was calculated by (each signal value/AVG value of controls) and is depicted as log2(normalized fold change. Significance was determined by performing a 2 tailed t-test between the fold change values for each antibody. Samples with a Coefficient of Variation >25% for technical triplicates were excluded from further analysis. Pathway analysis was done using Gene Ontology Pathway Analysis.

Protein Ribbon Structures:

The protein structure of SEMA7A was analyzed in PyMOL with an academic research license. Ribbon structure (purple) was created and modified to highlight the RGD motif (orange) and the antibody-binding site (green) in PyMOL.

Synergy Scores:

Bliss Synergy scores for two-drug combination treatments were calculated using Synergyfinder.org; scores ≤ -10 are considered antagonistic, between -10 and 10 are considered additive, and a score ≥ 10 is considered synergistic (37). Further details on the methods used can be found at https://synergyfinder.fimm.fi/synergy/synfin_docs/.

Novel drug treatments:

SmAb H1 (hybridoma): Mice were injected with SEMA7A protein and KLH peptide to enhance immune response. B cells from mouse spleens were fused with myeloma cells to create a hybridoma; positive hybridoma clones were selected and monoclonal antibodies were harvested. SmAb H1 Antibody binds to amino acids 381-392 of SEMA7A (green; SFigure 1G) (26).

rSmAb H1 (recombinant): The ExpiCHO-S expression system (Gibco) was used for the production of recombinant antibodies according to the manufacturer's protocol. After the 12 days of expression, the culture media were harvested by centrifugation, filtered through a 0.2-micron filter, and underwent affinity chromatography using MabSelect PrismA resin and the AKTA pure FPLC instrument for purification of recombinant monoclonal antibody.

GCT-007: GCT-007 is a pan PI3K inhibitor and was provided to us for these studies by Global Cancer Technology. (16776 Bernardo Center Drive #203, San Diego, CA 92128).

Statistical Analysis:

All quantitative and statistical analysis was performed using GraphPad Prism, and the methods of tests are labeled in the figure legends. The statistical tests used in this paper include unpaired two-tailed t-test, Pearson's correlation, and ordinary one-way ANOVA with Tukey's multiple comparisons test. All p-values were measured under two-tailed conditions. Significance was determined by a p-value less than 0.05. *$p<0.05$, **$p<0.01$, ***$p<0.001$ ****$p<0.0001$.

Data Availability:

The data generated in this study are available upon request from the corresponding author.

RESULTS

SEMA7A is expressed in ER+ breast cancer and is associated with decreased 5-year patient survival.

To test our hypothesis that SEMA7A predicts decreased response to therapy, and therefore poor prognosis, we used Kaplan-Meier Plotter(34) to examine 5-year survival for ER+ BC patients with high versus low tumor *SEMA7A* mRNA expression (Figure 1A-C). The probability of overall survival (OS) was significantly decreased for patients with high *SEMA7A* expression (Figure 1A), as well as distant metastasis-free survival (DMFS) (Figure 1B) and post-progression survival (PPS) (Figure 1C). Further, relapse-free survival (RFS) (Figure 1D) and DMFS (Figure 1E) was decreased in ER+ BC patients with high *SEMA7A* expression who had received endocrine therapy.

SEMA7A activates AKT signaling and binds to Integrins β1 and β4 via RGD in ER+ tumor cells.

To investigate differential protein and phospho-protein expression in ER+ MCF7 breast cancer cells transduced with an empty vector (EV) or SEMA7A overexpression (OE) vector, we utilized a reverse phase protein array (RPPA) (38). We confirmed SEMA7A overexpression via western blot prior to making RPPA lysates (SFigure 1A). We performed Gene Ontology (GO) Pathway Analysis on the RPPA data to identify prominent upregulated pathways in the SEMA7A OE lysates compared to EV and observed that signaling related to cell survival, including AKT, mTOR, and integrin signaling, was upregulated in SEMA7A OE cells (Figure 2A). Our RPPA data suggest that overexpression of SEMA7A leads to increased phospho-AKT (pAKT) mainly at serine 473 (S473) and not threonine 308 (T308) (Figure 2B; SFigure 1B). To validate that SEMA7A activates AKT signaling through pAKT (S473) in ER+ breast cancer cells, we measured pAKT (S473) and total AKT using immunoblot analysis on MCF7 EV and SEMA7A OE cells, or WT MCF7 treated with purified SEMA7A (rSEMA7A); the pAKT to AKT ratio was significantly higher in SEMA7A OE cells compared to EV and

rSEMA7A-treated cells compared to controls (SFigure 1C-D). Downstream AKT signaling targets, such as p-mTOR (S2448), p-P70S6K and Bcl-2, were also upregulated in SEMA7A OE (Figure 2C-E). Of note, PDK1, the kinase known to phosphorylate AKT at T308, was significantly downregulated in SEMA7A OE (Figure 2F). In concordance with these findings, we found that integrin-linked kinase (ILK), which phosphorylates AKT at serine 473 and bypasses PI3K, was upregulated in SEMA7A OE compared to controls (Figure 2G). We observed increases in several additional proteins, including integrin β1 **(**ITGB1), a known receptor for SEMA7A (20,39,40), as well as integrin β4 **(**ITGB4) (Figure 2H-I). Expression of *ITGB1* and *ITGB4* mRNA also weakly correlated with *SEMA7A* expression in the TCGA Breast Cancer Dataset (n=1247) (SFigure 1E-F). To investigate ITGB1 and ITGB4 as potential binding partners for SEMA7A in ER+ breast cancer cells, we performed co-immunoprecipitation (CoIP) in which SEMA7A protein was pulled down along with its binding partner(s). After CoIP, western blotting revealed binding of both ITGB1 and ITGB4 to SEMA7A, which was higher in SEMA7A OE cells compared to controls (Figure 2J). To investigate whether SEMA7A binds to integrins via its RGD (Arg-Gly-Asp) motif (SFigure 1G), which is known to facilitate integrin binding (41), we conducted CoIP using MCF7 SEMA7A OE lysates treated with PBS or RGDS (Arg-Gly-Asp-Ser) peptide, which inhibits RGD-integrin binding. Our results indicate that binding of SEMA7A to ITGB4 and ITGB1 was significantly reduced by the RGDS peptide (Figure 2K). These results were validated in an additional human ER+ breast cancer cell line, ZR75-1 (SFigure 1H).

SEMA7A-mediated activation of AKT depends on integrin binding in ER+ tumor cells.

After our results showed increased pAKT (S473) in SEMA7A OE and rSEMA7A-treated MCF7 cells (SFigure 1C-D). We chose to validate our results in a syngeneic ER+ cell line. We obtained TC11 and SSM2 cells, which are ER+ mouse mammary tumor cell lines (42,43)(generous gifts from Linda Schuler and Alexander Borowsky), and validated ERα expression compared to MCF7 (SFigure 2A). We also compared SEMA7A expression in the two cell lines to reveal that TC11 cells express slightly higher endogenous SEMA7A (SFigure 2B). To determine whether SEMA7A drives pAKT in the TC11 cell line, we compared cell lines stably transduced with shCtrl and shSEMA7A lentiviral vectors (shSEMA7A KD#1 and KD#2). SEMA7A expression was confirmed to be decreased in both KD vectors, with a larger decrease in KD#2 (SFigure 2C). As expected, knockdown of SEMA7A decreased pAKT levels, and the ratio of pAKT to AKT was decreased in a SEMA7A-dependent manner (Figure 3A). Additionally, we show that rSEMA7A or conditioned media from SEMA7A OE cells rescued the decrease in pAKT observed in the KD cells (Figure 3B). To further define whether AKT activation by SEMA7A occurs via SEMA7A-integrin binding, we treated TC11 cells with rSEMA7A, RGDS peptide or both, and measured pAKT/AKT expression (Figure 3C). Although the RGDS peptide alone inhibited pAKT levels, our results also show that rSEMA7A increased pAKT, and this effect was inhibited by the RGDS peptide (Figure 3C). We observed similar results with the RGDS in two additional ER+ cell lines, MCF7 and ZR751 (SFigure 2D-E).

SEMA7A+ tumor growth is inhibited by combination treatment with endocrine therapy and PI3K inhibitors.

Since there are no clinically available integrin or ILK inhibitors, we investigated other therapeutic strategies to inhibit SEMA7A-mediated signaling. Further, increased pAKT levels in SEMA7A OE cells suggest a potential increase in PI3K signaling activity (44). Thus, we hypothesized that SEMA7A+ ER+ BC cells would exhibit increased sensitivity to treatment with PI3K inhibitors (PI3Ki). To test this hypothesis, we determined the 50% inhibitory concentration (IC50) for alpelisib (p110α inhibitor; SFigure 3A) and GCT-007 (pan-PI3K inhibitor; SFigure 3B) in MCF7 EV and SEMA7A OE cells. The IC50 of alpelisib and GCT-007 in SEMA7A OE cells was lower, suggesting increased susceptibility to PI3Ki in SEMA7A-expressing tumor cells. We also examined sensitivity to PI3Ki in TC11 shSEMA7A #2 KD cells compared to controls (SFigure 3C-D). In support of our conclusion, cell viability assays revealed that inhibition by both alpelisib and GCT-007 is greater in SEMA7A OE cells, compared to controls (SFigure 3E). We also confirmed that pAKT expression is reduced by both PI3Ki treatments in MCF7 and TC11 (SFigure 3F-G) cells.

Since PI3K inhibition is utilized clinically in conjunction with endocrine therapy for ER+ breast cancers, we aimed to evaluate whether a combination of endocrine therapy and PI3K inhibition (PI3Ki) would be more effective than either treatment alone in SEMA7A-expressing tumors. Based on previous literature (2) and our IC50 curves (SFigure 3A-D; SFigure 4A-B), we treated ER+ TC11 cells with fulvestrant, alpelisib, or the combination and measured cell viability to reveal that fulvestrant alone had minimal effect, while single-agent alpelisib and GCT-007 resulted in a moderate reduction in cell viability, and the combination treatments were the most effective (Figure 4A-B). Similar results were observed with the combination of fulvestrant plus alpelisib or GCT-007 in another ER+ cell line, ZR75-1 (SFigure 4C-D). Notably, TC11 tumor cells are known to exhibit resistance to tamoxifen (42). Therefore, we also tested the combination of tamoxifen and each PI3Ki in TC11 cells; our findings show that tamoxifen alone has minimal effect, whereas the combination significantly reduced cell viability compared to control, and more so than either single agent (Figure 4C-D). Following *in vitro* synergy assays, Bliss synergy scores were calculated for the treatment combinations of fulvestrant (Figure 4E-F) and tamoxifen (Figure 4G-H) with PI3K inhibitors. To evaluate the combination of endocrine therapy and PI3K inhibition *in vivo*, MCF7 SEMA7A OE tumor-bearing NCG mice were treated with fulvestrant alone or in conjunction with alpelisib or GCT-007, resulting in a greater reduction of tumor growth with the combination treatments compared to fulvestrant alone (SFigure 4E-F). Mouse weights were monitored, and no toxicities were observed with either PI3K inhibitor (SFigure G-H). In data from the manufacturer, GCT-007 performs better in mice with an intact immune system (unpublished observations). Therefore, to test our combination treatments in an ER+, estrogen-responsive (42)(SFigure 4I), immune-competent model, TC11 tumor-bearing FVB/N mice were treated with tamoxifen, GCT-007, or the combination; the combination was most effective at inhibiting tumor growth compared to either single agent or controls (Figure 4I). Mouse weights were monitored, and no toxicities were observed (SFigure 4J).

Inhibition of SEMA7A using a monoclonal antibody (SmAb H1) effectively reduces tumor growth and AKT signaling in ER+ BC.

We next tested our hypothesis that resistance to endocrine therapy, mediated by SEMA7A (2), could be reversed by direct targeting of SEMA7A using our novel anti-SEMA7A monoclonal antibody (SmAb H1) that we have previously shown to have efficacy in ER-negative models of breast cancer(29,30). Our *in vitro* BioSpa live imaging assay results show that cell viability is reduced by 1 μM SmAb H1 over time in MCF7 SEMA7A OE cells, but not in EV controls (Figure 5A). The IC50 for SmAb H1 is also lower in SEMA7A OE compared to controls (SFigure 5A), suggesting SmAb H1 is specific to SEMA7A-expressing cells. Previous studies from our lab have confirmed binding specificity of SmAb H1 to SEMA7A protein via ELISA (26). In contrast, TC11 SEMA7A knockdown cells (shSEMA7A KD#2) showed no response to SmAb H1, whereas TC11 control (shCtrl) cells were sensitive to SmAb H1 *in vitro* (Figure 5B). Our previous studies suggest that SmAbH1 is not efficacious in immune-compromised hosts (29), thus, we evaluated SmAb H1 in the TC11 model *in vivo* (SFigure 5B-D). We observed inhibition of tumor growth in SmAb H1-treated tumors only (SFigure 5B-C). Mouse weights were monitored, and no toxicities were observed (SFigure 5D). We validated these findings in the SSM2/129Sv-E model, an additional ER+ syngeneic model (45) with endogenous SEMA7A expression (SFigure 2B, SFigure 5E). To further look at specificity of SmAb H1, we implanted either TC11 shCtrl or shSEMA7A KD#2 tumor cells into FVB-N mice and initiated treatment after tumor establishment. We observed that SmAb H1 inhibited tumor growth compared to the IgG control (Figure 5C), and this effect was specific to SEMA7A-expressing shCtrl tumors only (Figure 5C). Tumor volume calculated at study endpoint and tumor weight were significantly reduced only in the TC11 shCtrl tumors treated with SmAb H1 (Figure 5D-E). To confirm a SEMA7A integrin-mediated mechanism *in vivo*, we performed IHC staining on control and SmAb H1-treated TC11 tumors to show that activated integrin β1 (9EG7), integrin β4, and SEMA7A expression were reduced in the SmAb H1-treated group (Figure 5F, SFigure 5F-I). Percent positive tumor IHC staining was quantified and showed reduced ITGB1 (9EG7), ITGB4 and SEMA7A (Figure 5 G-I). Finally, we performed RPPA analysis (RPPA-2) of lysates made from IgG-treated and SmAb H1-treated TC11 and SSM2 tumors to reveal decreased protein expression of pAKT (S473) as well as downstream AKT targets, such as p-P70S6K and Bcl-2, in the SmAb H1-treated group (Figure 5J-K, SFigure 5J-M). These data were validated in

the SSM2 model; showing even further reduction in fold change of several AKT targets; p-P70S6K, p-mTOR(S2448), and Bcl-2 (Figure L-N, SFigure 5N-P).

Combination treatment with fulvestrant and SmAb H1 reduces SEMA7A+ ER+ tumor growth.

To test the hypothesis that the combination of SmAb H1 and fulvestrant may benefit patients, we tested cell viability in TC11 and MCF7 cell lines. TC11 shCtrl cell viability was inhibited by SmAb H1 alone, and even more so by combination of fulvestrant and SmAb H1, whereas TC11 shSEMA7A KD#2 viability was not affected (Figure 6A). Further, treatment of MCF7 EV and SEMA7A OE cells with fulvestrant, SmAb H1, or the combination showed that SEMA7A OE cells respond positively to SmAb H1 as a single agent and even more robustly to the combination of fulvestrant and SmAb H1, while control cells do not (SFigure 6A). Additionally, EV cells exhibit a moderate response to fulvestrant alone, while SEMA7A OE cells do not (SFigure 6A). These results were validated in SSM2 and ZR75-1 cells (SFigure 6B-C). In contrast, TC11 shSEMA7A cells displayed increased sensitivity to fulvestrant alone (Figure 6A), suggesting that the loss of SEMA7A may re-sensitize TC11 tumor cells to fulvestrant. We also calculated synergy scores for fulvestrant in combination with SmAb H1 in TC11 cells (Figure 6B). The synergy of SmAb H1 with fulvestrant was greater than with tamoxifen (SFigure 6D), thus we moved forward with fulvestrant. To test this hypothesis *in vivo,* TC11 shCtrl and shSEMA7A KD#2 tumor cells were implanted into FVB/N mice and groups with Vehicle, IgG1, fulvestrant, SmAb H1, or the combination of fulvestrant and SmAb H1. Tumor growth of shCtrl tumors was reduced by SmAbH1 and the combination therapy, but not the controls or fulvestrant alone (Figure 6C). Consistent with our hypothesis, growth of TC11 shSEMA7A tumors was not affected by SmAb H1 alone, but was reduced by fulvestrant and the combination therapy (Figure 6D). Prior to repeating this *in vivo* experiment, we tested a newer version of anti-SEMA7A antibody, rSmAb H1-P for range of reactivity and specificity via IC50 and ELISA assay (SFigure 6E-F). Synergy results revealed that rSmAb H1-P and fulvestrant are synergistic *in vitro,* similarly to SmAb H1 and fulvestrant (SFigure 6G). Then we repeated the *in vivo* experiment with rSmAb H1-P and fulvestrant; images of harvested tumors show visibly smaller tumors in the rSmAb H1-P-treated and combination-treated groups compared to controls or fulvestrant alone (Figure 6E). Mouse weights were monitored (SFigure 6H), and a 6-chemistry toxicity panel was run on mouse plasma and showed no differences between rSmAb H1-P-treated treatment and control-treated mice (SFigure 6I-N).

DISCUSSION

Our findings provide premise for treating patients with SEMA7A+ breast cancer with more targeted therapies, including those that target of PI3K and/or directly target SEMA7A. Given our previous studies that have shown poor relapse-free survival rates in both ER+ and ER- breast cancer patients (2), clinical trials informed by our data stand to impact thousands of patients annually. While we did not see increased PI3K or PDK1, we saw increased pAKT, ILK and downstream targets of AKT, so we think ILK activation of AKT is also playing a role. Since there are no clinically available integrin or ILK inhibitors, we chose to start with PI3K inhibitors to inhibit the SEMA7A-AKT pathway. Clinical use of alpelisib is currently approved for patients with an E545K mutation in *PIK3CA* that causes constitutive activation of the PI3K p110α subunit (46). However, we hypothesize that even in the absence of the *PIK3CA* E545K mutation, high SEMA7A expression can cause hyperactivation of PI3K including p110α, thus SEMA7A-expressing tumors may be sensitive to alpelisib (47)(Figure 3,4). GCT-007, a pan-PI3K inhibitor that has shown preclinical efficacy in glioblastoma, is not approved yet for clinical use, but our results suggest it may be efficacious in breast cancer patients as well (Figure 3, 4). Limitations of the clinical applicability of our study include the known toxicities observed in some patients including hyperglycemia, rash, and diarrhea (48), and while we saw no overt toxicities in our mouse studies, the potential toxicities of GCT-007 in humans is unknown.

Previous studies implicated ITGB1as a receptor for SEMA7A on cancer cells and other cell types, our findings suggest that SEMA7A binds to both ITGB1 and ITGB4 in ER+ breast cancer cells (Figure 2). We also provide evidence that the RGD motif within SEMA7A mediates binding to β-integrins as it can be blocked with an RGDS peptide (Figure 2). Furthermore, our findings with the RGDS blocking peptide suggest that SEMA7A

enhances phosphorylation and activation of AKT specifically through integrins (Figure 3), which were previously shown to undergo conformational changes when bound by an RGD motif leading to intracellular activation of signaling pathways such as PI3K/AKT, Fak, and MAPK/ERK (49). Further, it has been previously shown that ITGB1 upstream of PI3K and MAPK signaling can facilitate endocrine therapy resistance in breast cancer (50); thus blocking this pathway is a potential way to overcome endocrine therapy resistance. Limitations of the current study include that the synthetic RGDS peptide may have also caused non-specific integrin inhibition beyond that attributed to SEMA7A. Further, while the RGD motif in SEMA7A is known, the protein folding structure of SEMA7A when bound versus unbound to integrins remains unknown.

Our results suggest that direct inhibition of SEMA7A via our monoclonal antibody, SmAb H1, is a promising therapeutic strategy that should be further investigated with additional pre-clinical studies to enable progression to first in human clinical trials. While the combination of fulvestrant and SmAb H1 did reach statistical significance compared to SmAb H1 alone, it is important to note that SmAb H1 did not appear to interfere with fulvestrant, which is utilized clinically for ER+ breast cancers and at study end the tumors were visibly smaller in the combination-treated group (Figure 6E). A limitation of our study is the use of mouse cell lines for the in vivo models instead of human. We deliberately chose the TC11 and SSM2 models to test SmAb H1 because they are immunocompetent and we have recently published that SmAb H1 activates anti-tumor T cell responses and does not work in T cell deficient mice(26).

We conclude that inhibition of SEMA7A mediated signaling in breast cancer, both direct and indirect, are promising clinical treatment avenues that should be further investigated particularly in patients with recurrent disease despite endocrine therapies. Furthermore, our previous results suggest that SEMA7A positive tumors will not respond to CDK4/6 inhibition, which is FDA approved for ER+ breast cancer patients. Additionally, our results suggest that patients with ER+ BC may benefit from a diagnostic test that quantifies SEMA7A expression as we have published a threshold of SEMA7A expression by immunostaining fixed tissues that can predict for relapse in a small patient dataset(17). If such a diagnostic existed, patients with SEMA7A+ tumors could receive a SEMA7A-targeted therapy similar to patients with HER2+ disease that are treated with trastuzumab. Future directions could also include the development and optimization of a minimally invasive SEMA7A-detecting diagnostic (blood) test, which we have initiated. However, further investigation is needed to determine whether SEMA7A levels in tumors correlate with levels in patient serum samples. Meanwhile, AKT inhibitors such as capivasertib and ipatasertib, mTOR inhibitors such as everolimus, and other PI3K inhibitors such as a p110δ inhibitors (idelalisib) could be explored in our SEMA7A+ER+BC models to optimize available treatment combinations. Moreover, we have published that venetoclax can slow tumor growth in pre-clinical models and our current RPPA results confirm decreased Bcl-2 levels; thus, combination of SmAbH1 and venetoclax should also be explored. Cumulatively, our current and previous studies suggest a unique and druggable aspect in the biology of SEMA7A positive breast cancers that could transform treatment options for thousands of patients annually.

ACKNOWLEDGEMENTS

- Technical support
    - Lyons lab: Crump, L., Cozzens, L., Kines, K., Elder, A., Becks, A.
    - Sarah Tarullo Plymouth State University
    - Porter lab: Porter, W., Wyatt, G. (A&M)
- Provided Reagents:
    - Global Cancer Technology
    - Novartis
- Virginia Borges clinical mentor
- Committee members: Sartorius, C., Bitler, B., Fantauzzo, K., Tentler, J., Richer, J., Sherbenou, D.
- Mike Oliphant experimental advice

- NIH/NCATS Colorado CTSA Grant Number TL1 TR002533 (RS)
- NIC R01CA282900-01 and R01HD108335-01A1 to TL
- SPARK/REACH Program NIH: U01HL152405 and OEIDIT/AIA: MA 2021-2028 to TL
- ABN Ohana Gates Grubstake Award to TL
- DOM Outstanding Early Career Scholars Program
- UCCC and DOM ASPIRE to TL
- Men for the Cure PO1 pilot grant to TL
- University of Colorado Cancer Center Support Grant #P30CA046934 (RS 2024)
    - Anh Le, Steve Anderson and the University of Colorado Anschutz CTSR (Cell Technologies Shared Resource)
    - University of Colorado Anschutz CPSR (Comparative Pathology Shared Resource)
- Cancer Prevention & Research Institute of Texas Core Facility Support Awards (PR210227, PI: Dean Edwards)
    - Baylor College of Medicine Antibody-Based Proteomics Core
        - Dean Edwards
        - Shixia Huang

REFERENCES

1. ACS. 2024 American Cancer Society: Cancer Facts and Figures 2024. In American Cancer Society <https://www.cancer.org/research/cancer-facts-statistics/all-cancer-facts-figures/2024-cancer-facts-figures.html>.
2. Crump LS, Wyatt GL, Rutherford TR, Richer JK, Porter WW, Lyons TR. Hormonal Regulation of Semaphorin 7a in ER⁺ Breast Cancer Drives Therapeutic Resistance. Cancer Research **2021**;81:187-98
3. Pan H, Gray R, Braybrooke J, Davies C, Taylor C, McGale P*, et al.* 20-Year Risks of Breast-Cancer Recurrence after Stopping Endocrine Therapy at 5 Years. N Engl J Med **2017**;377:1836-46
4. Pasterkamp RJ, Peschon JJ, Spriggs MK, Kolodkin AL. Semaphorin 7A promotes axon outgrowth through integrins and MAPKs. Nature **2003**;424:398-405
5. Bao ZZ, Jin Z. Sema3D and Sema7A have distinct expression patterns in chick embryonic development. Dev Dyn **2006**;235:2282-9
6. Kohler D, Granja T, Volz J, Koeppen M, Langer HF, Hansmann G*, et al.* Red blood cell-derived semaphorin 7A promotes thrombo-inflammation in myocardial ischemia-reperfusion injury through platelet GPIb. Nat Commun **2020**;11:1315
7. Manini I, Ruaro ME, Sgarra R, Bartolini A, Caponnetto F, Ius T*, et al.* Semaphorin-7A on Exosomes: A Promigratory Signal in the Glioma Microenvironment. Cancers (Basel) **2019**;11
8. Kinehara Y, Nagatomo I, Koyama S, Ito D, Nojima S, Kurebayashi R*, et al.* Semaphorin 7A promotes EGFR-TKI resistance in EGFR mutant lung adenocarcinoma cells. JCI Insight **2018**;3
9. Xie J, Wang H. Semaphorin 7A as a potential immune regulator and promising therapeutic target in rheumatoid arthritis. Arthritis Res Ther **2017**;19:10
10. Vaidya B, Patel R, Muth A, Gupta V. Exploitation of Novel Molecular Targets to Treat Idiopathic Pulmonary Fibrosis: A Drug Discovery Perspective. Curr Med Chem **2017**;24:2439-58
11. Garcia-Areas R, Libreros S, Simoes M, Castro-Silva C, Gazaniga N, Amat S*, et al.* Suppression of tumor-derived Semaphorin 7A and genetic ablation of host-derived Semaphorin 7A impairs tumor progression in a murine model of advanced breast carcinoma. Int J Oncol **2017**;51:1395-404
12. Gutierrez-Franco A, Eixarch H, Costa C, Gil V, Castillo M, Calvo-Barreiro L*, et al.* Semaphorin 7A as a Potential Therapeutic Target for Multiple Sclerosis. Mol Neurobiol **2016**

13. Roth JM, Kohler D, Schneider M, Granja TF, Rosenberger P. Semaphorin 7A Aggravates Pulmonary Inflammation during Lung Injury. PLoS One **2016**;11:e0146930
14. Tarullo SE, Hill RC, Hansen KC, Behbod F, Borges VF, Nelson AC*, et al.* Postpartum breast cancer progression is driven by semaphorin 7a-mediated invasion and survival. Oncogene **2020**;39:2772-85
15. Rutherford TR, Elder AM, Lyons TR. Anoikis resistance in mammary epithelial cells is mediated by semaphorin 7a. Cell Death Dis **2021**;12:872
16. Black SA, Nelson AC, Gurule NJ, Futscher BW, Lyons TR. Semaphorin 7a exerts pleiotropic effects to promote breast tumor progression. Oncogene **2016**;35:5170-8
17. Borges VF, Hu J, Young C, Maggard J, Parris HJ, Gao D*, et al.* Semaphorin 7a is a biomarker for recurrence in postpartum breast cancer. npj Breast Cancer **2020**;6:56
18. Elder AM, Tamburini BAJ, Crump LS, Black SA, Wessells VM, Schedin PJ*, et al.* Semaphorin 7A Promotes Macrophage-Mediated Lymphatic Remodeling during Postpartum Mammary Gland Involution and in Breast Cancer. Cancer Res **2018**;78:6473-85
19. Kines KaF, Heather and Elder, Alan and Cozzens, Lauren and Strugar, Zachary and Porter, Weston and Borges, Virginia and Lyons, Traci, . Aging-Induced Semaphorin 7a Promotes Tgfβ1-Mediated Cell Plasticity and Breast Tumor Metastases. **2024**
20. Suzuki K, Kumanogoh A, Kikutani H. Semaphorins and their receptors in immune cell interactions. Nat Immunol **2008**;9:17-23
21. Duarte A, Silveira GG, Soave DF, Costa JPO, Silva AR. The Role of the LY294002 - A Non-Selective Inhibitor of Phosphatidylinositol 3-Kinase (PI3K) Pathway- in Cell Survival and Proliferation in Cell Line SCC-25. Asian Pac J Cancer Prev **2019**;20:3377-83
22. Yang SX, Polley E, Lipkowitz S. New insights on PI3K/AKT pathway alterations and clinical outcomes in breast cancer. Cancer Treat Rev **2016**;45:87-96
23. Bostner J, Karlsson E, Pandiyan MJ, Westman H, Skoog L, Fornander T*, et al.* Activation of Akt, mTOR, and the estrogen receptor as a signature to predict tamoxifen treatment benefit. Breast Cancer Res Treat **2013**;137:397-406
24. Burris HA, 3rd. Overcoming acquired resistance to anticancer therapy: focus on the PI3K/AKT/mTOR pathway. Cancer Chemother Pharmacol **2013**;71:829-42
25. Chen H, Mingming C, Pengcheng G, Xiangzhong Z, Ganggang L, Liting W*, et al.* GDC-0941 activates integrin linked kinase (ILK) expression to cause resistance to GDC-0941 in breast cancer by the tumor necrosis factor (TNF)-α signaling pathway. Bioengineered **2022**;13:10944-55
26. Elder AM, Fairchild HR, Kines KT, Cozzens LM, Becks AR, Slansky JE*, et al.* Semaphorin7A and PD-L1 cooperatively drive immunosuppression during mammary involution and breast cancer. Cell Rep **2025**;44:115676
27. Czopik AK, Bynoe MS, Palm N, Raine CS, Medzhitov R. Semaphorin 7A Is a Negative Regulator of T Cell Responses. Immunity **2006**;24:591-600
28. Gómez Tejeda Zañudo J, Mao P, Alcon C, Kowalski K, Johnson GN, Xu G*, et al.* Cell Line-Specific Network Models of ER(+) Breast Cancer Identify Potential PI3Kα Inhibitor Resistance Mechanisms and Drug Combinations. Cancer Res **2021**;81:4603-17
29. Kines KaF, Heather and Elder, Alan and Cozzens, Lauren and Strugar, Zachary and Porter, Weston and Borges, Virginia and Lyons, Traci, . Aging-Induced Semaphorin 7a Promotes Tgfβ1-Mediated Cell Plasticity and Breast Tumor Metastases. Cell Press Sneak Peak **2024**
30. Elder AM, Fairchild HR, Kines KT, Cozzens LM, Becks AR, Lyons TR. Semaphorin7A and PD-L1 cooperatively drive immunosuppression during mammary involution and breast cancer. bioRxiv **2025**:2025.01.03.631229
31. Schneider CA, Rasband WS, Eliceiri KW. NIH Image to ImageJ: 25 years of image analysis. Nat Methods **2012**;9:671-5

32. DeRose YS, Gligorich KM, Wang G, Georgelas A, Bowman P, Courdy SJ*, et al*. Patient-derived models of human breast cancer: protocols for in vitro and in vivo applications in tumor biology and translational medicine. Curr Protoc Pharmacol **2013**;Chapter 14:Unit14 23
33. Massarweh S, Osborne CK, Creighton CJ, Qin L, Tsimelzon A, Huang S*, et al*. Tamoxifen resistance in breast tumors is driven by growth factor receptor signaling with repression of classic estrogen receptor genomic function. Cancer Res **2008**;68:826-33
34. Gyorffy B. Survival analysis across the entire transcriptome identifies biomarkers with the highest prognostic power in breast cancer. Comput Struct Biotechnol J **2021**;19:4101-9
35. Goldman MJ, Craft B, Hastie M, Repecka K, McDade F, Kamath A*, et al*. Visualizing and interpreting cancer genomics data via the Xena platform. Nat Biotechnol **2020**;38:675-8
36. Coarfa C, Grimm SL, Rajapakshe K, Perera D, Lu HY, Wang X*, et al*. Reverse-Phase Protein Array: Technology, Application, Data Processing, and Integration. J Biomol Tech **2021**
37. Zheng S, Wang W, Aldahdooh J, Malyutina A, Shadbahr T, Tanoli Z*, et al*. SynergyFinder Plus: Toward Better Interpretation and Annotation of Drug Combination Screening Datasets. Genomics Proteomics Bioinformatics **2022**;20:587-96
38. Davis JB, Andes S, Espina V. Reverse Phase Protein Arrays. Methods Mol Biol **2021**;2237:103-22
39. Huang J, Zhao C, Zhang S. Semaphorin 7A promotes endothelial permeability and inflammation via plexin C1 and integrin β1 in Kawasaki disease. BMC Pediatr **2024**;24:285
40. Suzuki K, Okuno T, Yamamoto M, Pasterkamp RJ, Takegahara N, Takamatsu H*, et al*. Semaphorin 7A initiates T-cell-mediated inflammatory responses through alpha1beta1 integrin. Nature **2007**;446:680-4
41. Ludwig BS, Kessler H, Kossatz S, Reuning U. RGD-Binding Integrins Revisited: How Recently Discovered Functions and Novel Synthetic Ligands (Re-)Shape an Ever-Evolving Field. Cancers (Basel) **2021**;13
42. Jallow F, O'Leary KA, Rugowski DE, Guerrero JF, Ponik SM, Schuler LA. Dynamic interactions between the extracellular matrix and estrogen activity in progression of ER+ breast cancer. Oncogene **2019**;38:6913-25
43. Mori H, Chen JQ, Cardiff RD, Pénzváltó Z, Hubbard NE, Schuetter L*, et al*. Pathobiology of the 129:Stat1 (-/-) mouse model of human age-related ER-positive breast cancer with an immune infiltrate-excluded phenotype. Breast Cancer Res **2017**;19:102
44. Mayer IA, Arteaga CL. The PI3K/AKT Pathway as a Target for Cancer Treatment. Annu Rev Med **2016**;67:11-28
45. Mori H, Chen JQ, Cardiff RD, Pénzváltó Z, Hubbard NE, Schuetter L*, et al*. Pathobiology of the 129:Stat1−/− mouse model of human age-related ER-positive breast cancer with an immune infiltrate-excluded phenotype. Breast Cancer Research **2017**;19:102
46. Chang DY, Ma WL, Lu YS. Role of Alpelisib in the Treatment of PIK3CA-Mutated Breast Cancer: Patient Selection and Clinical Perspectives. Ther Clin Risk Manag **2021**;17:193-207
47. Armaghani AJ, Han HS. Alpelisib in the Treatment of Breast Cancer: A Short Review on the Emerging Clinical Data. Breast Cancer (Dove Med Press) **2020**;12:251-8
48. Wilhoit T, Patrick JM, May MB. Alpelisib: A Novel Therapy for Patients With PIK3CA-Mutated Metastatic Breast Cancer. J Adv Pract Oncol **2020**;11:768-75
49. Nieberler M, Reuning U, Reichart F, Notni J, Wester HJ, Schwaiger M*, et al*. Exploring the Role of RGD-Recognizing Integrins in Cancer. Cancers (Basel) **2017**;9
50. Pontiggia O, Sampayo R, Raffo D, Motter A, Xu R, Bissell MJ*, et al*. The tumor microenvironment modulates tamoxifen resistance in breast cancer: a role for soluble stromal factors and fibronectin through β1 integrin. Breast Cancer Res Treat **2012**;133:459-71

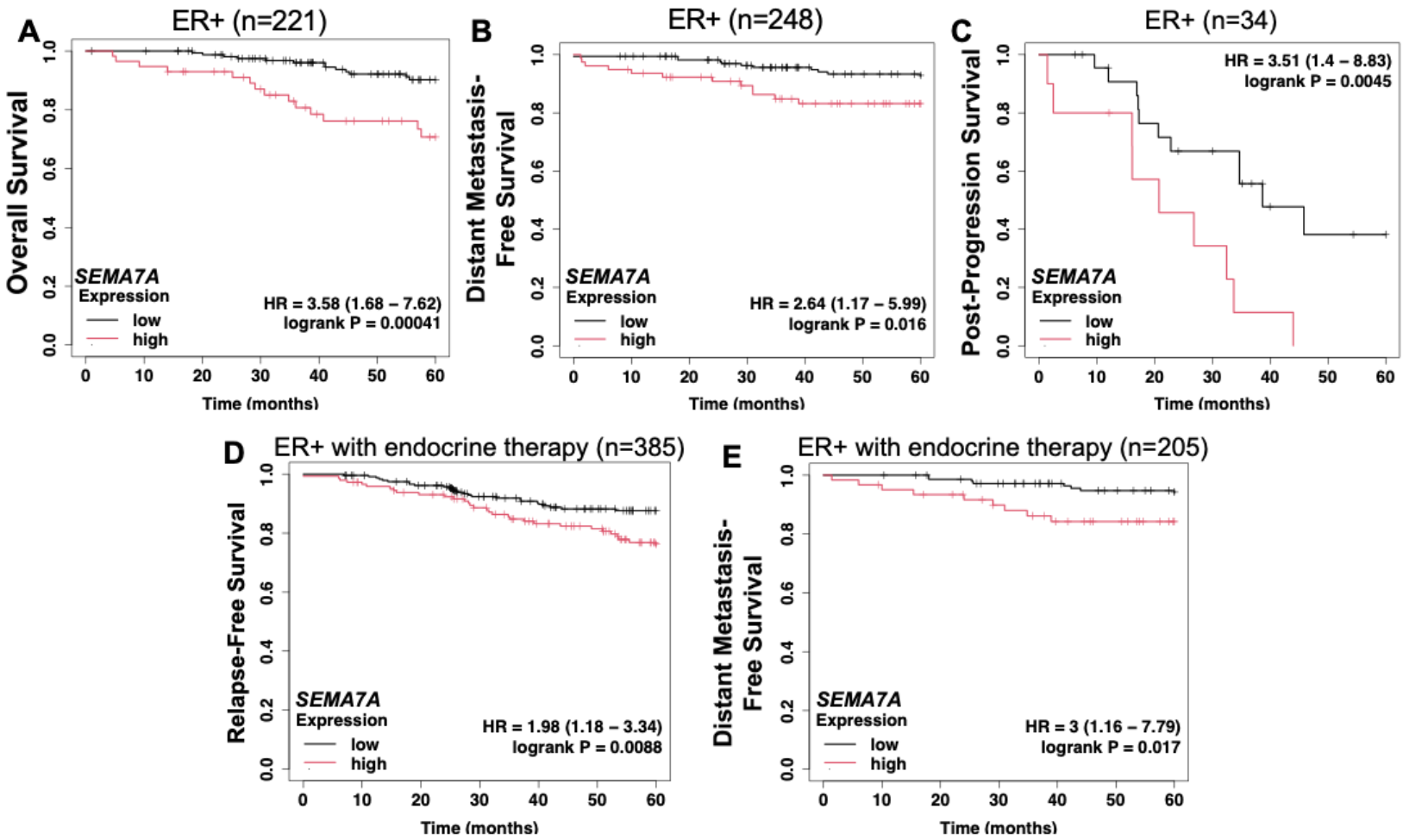

Figure 1. SEMA7A is expressed in ER+ breast cancer and is associated with decreased 5-year patient survival.

Figure 1. SEMA7A is expressed in ER+ breast cancer and is associated with decreased 5-year patient survival.

Survival analysis was done via Kaplan-Meier Plotter, which was assessed for *SEMA7A* mRNA expression levels in breast cancer patients in the ER+ subtype dataset (n=3499). Data are shown as KM plots; curves are stratified by *SEMA7A* high (red) and low (black) expression. Hazard ratios (HR) and log-rank p-values are included.

A) Overall survival; ER+ subtype (OS; n=221).

B) Distant metastasis-free survival; ER+ subtype (DMFS; n=248).

C) Post-progression survival; ER+ subtype (PPS; n=34).

Further analysis was done within the ER+ subtype to include only patients who had received endocrine therapy (n=1831).

D) Relapse-free survival; ER+ and received endocrine therapy (RFS; n=385).

E) Distant metastasis-free survival: ER+ and received endocrine therapy (DMFS; n=205).

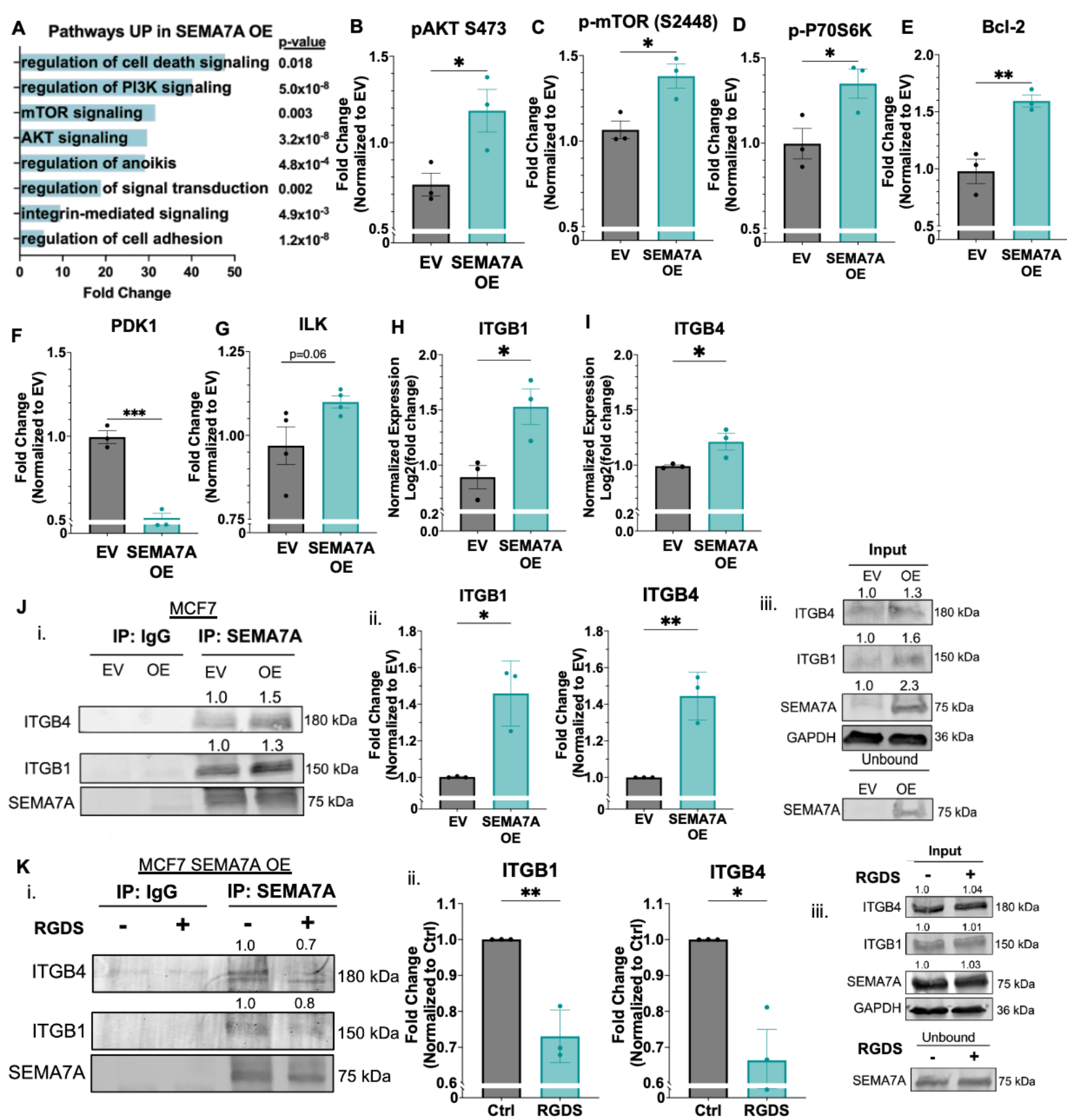

Figure 2. SEMA7A activates AKT signaling and binds to Integrins β1 and β4 via RGD in ER+ tumor cells.

Figure 2. SEMA7A activates AKT signaling and binds to Integrins β1 and β4 via RGD in ER+ tumor cells.

A) Gene Ontology (GO) Pathway Analysis of RPPA results, showing top pathways upregulated in MCF7 SEMA7A OE cell lysates, as fold change compared to EV, $p<0.05$.

B) Phospho-AKT (S473) protein expression in MCF7 EV and SEMA7A OE lysates from RPPA-1 data. Two-tailed unpaired t-test.

C) Phospho-mTOR (S2448) protein expression in MCF7 EV and SEMA7A OE lysates from RPPA-1 data. Two-tailed unpaired t-test.

D) Phospho-P70S6K protein expression in MCF7 EV and SEMA7A OE lysates from RPPA-1 data. Two-tailed unpaired t-test.

E) Bcl-2 protein expression in MCF7 EV and SEMA7A OE lysates from RPPA-1 data. Two-tailed unpaired t-test.

F) PDK1 protein expression in MCF7 EV and SEMA7A OE lysates from RPPA-1 data. Two-tailed unpaired t-test.

G) ILK protein expression in MCF7 EV and SEMA7A OE lysates from RPPA-1 data. Two-tailed unpaired t-test.

H) ITGB1 protein expression in MCF7 EV and SEMA7A OE lysates from RPPA-1 data. Two-tailed unpaired t-test.

I) ITGB4 protein expression in MCF7 EV and SEMA7A OE lysates from RPPA-1 data. Two-tailed unpaired t-test.

J) i. Immunoblot for ITGB4, ITGB1, and SEMA7A in elutions following CoIP of MCF7 EV and SEMA7A OE lysates for IgG or SEMA7A. ii. Quantification of IP lanes in (i), shown as fold change compared to EV. Two-tailed unpaired t-test. iii. Immunoblot for ITGB4, ITGB1, SEMA7A and GAPDH in MCF7 EV or SEMA7A OE lysates (input) and for SEMA7A in the unbound sample.

K) i. Immunoblot for ITGB4, ITGB1, and SEMA7A in elutions following CoIP of MCF7 lysates for IgG or SEMA7A, after treatment with PBS (-) or 50 μM RGDS (+). ii. Quantification of IP lanes in (i), shown as fold change compared to control. Two-tailed unpaired t-test. iii. Immunoblot for ITGB4, ITGB1, SEMA7A, and GAPDH in MCF7 SEMA7A OE lysates after treatment with PBS or 50 μM RGDS peptide for 1 hour (input), and for SEMA7A in the unbound sample.

Error bars are mean +/- SD. *$p<0.05$, **$p<0.01$, ***$p<0.001$, ****$p<0.0001$.

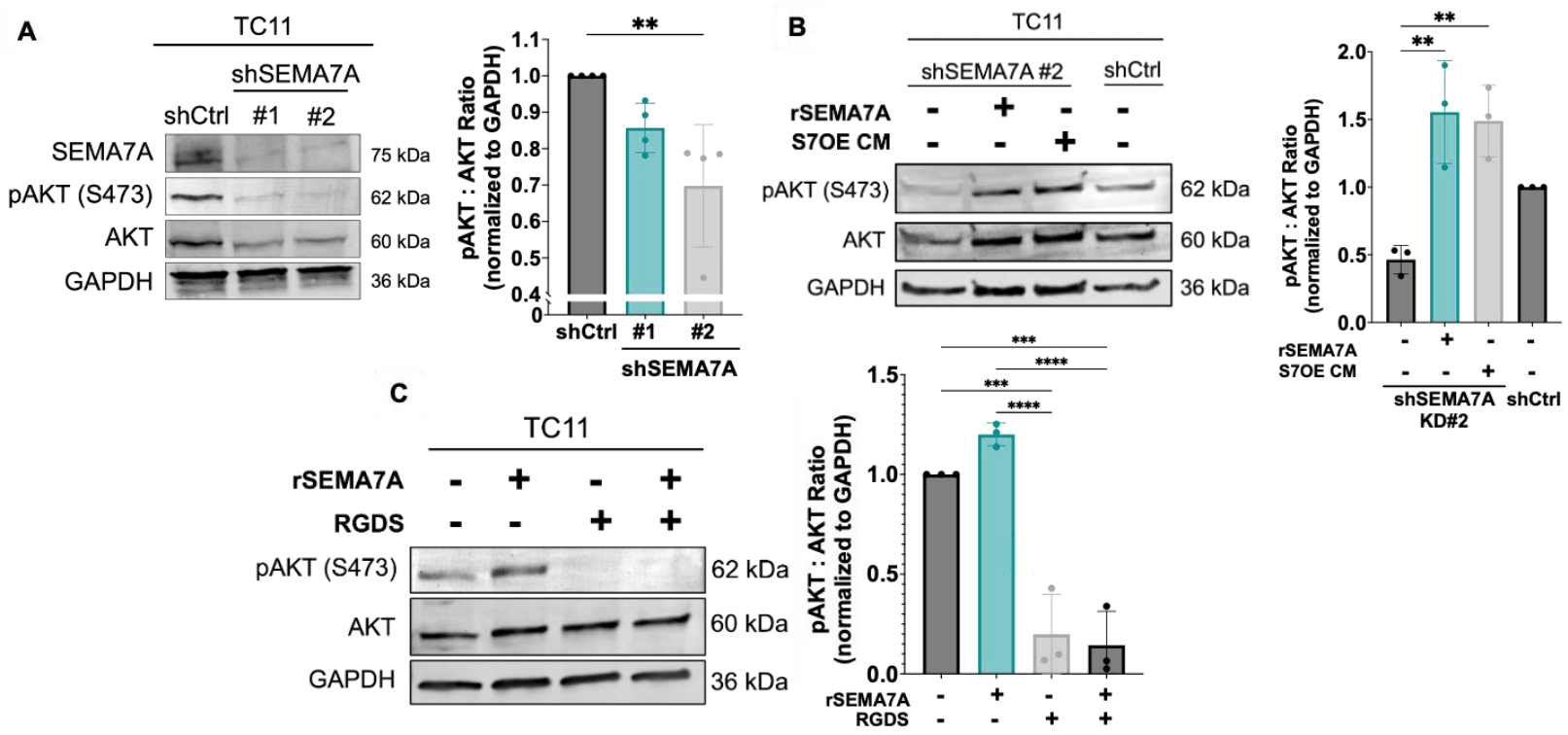

Figure 3. SEMA7A-mediated activation of AKT is dependent on RGD binding in ER+ tumor cells.

Figure 3. SEMA7A-mediated activation of AKT depends on integrin binding in ER+ tumor cells.

A) Representative immunoblot for pAKT (S473), AKT and GAPDH in TC11 shCtrl and shSEMA7A (KD#1 and KD#2) cell lines. Bar graph: ratio of pAKT to total AKT. Ordinary one-way ANOVA with Tukey's multiple comparisons test.

B) Representative immunoblot for pAKT (S473), AKT and GAPDH in TC11 shCtrl and shSEMA7A KD#2 cell lines after treatment for 24 hours with 20 μg/mL purified rSEMA7A, or conditioned media from SEMA7A OE cells (S7OE CM). Bar graph: ratio of pAKT to total AKT. Ordinary one-way ANOVA with Tukey's multiple comparisons test.

C) Representative immunoblot for pAKT (S473), AKT and GAPDH in TC11 WT cell lysates after treatment for 1 hour with 20 μg/mL rSEMA7A, 50 μM RGDS peptide, or both. Bar graph: ratio of pAKT to total AKT. Ordinary one-way ANOVA with Tukey's multiple comparisons test.

Error bars are mean +/- SD. *$p<0.05$, **$p<0.01$, ***$p<0.001$, ****$p<0.0001$.

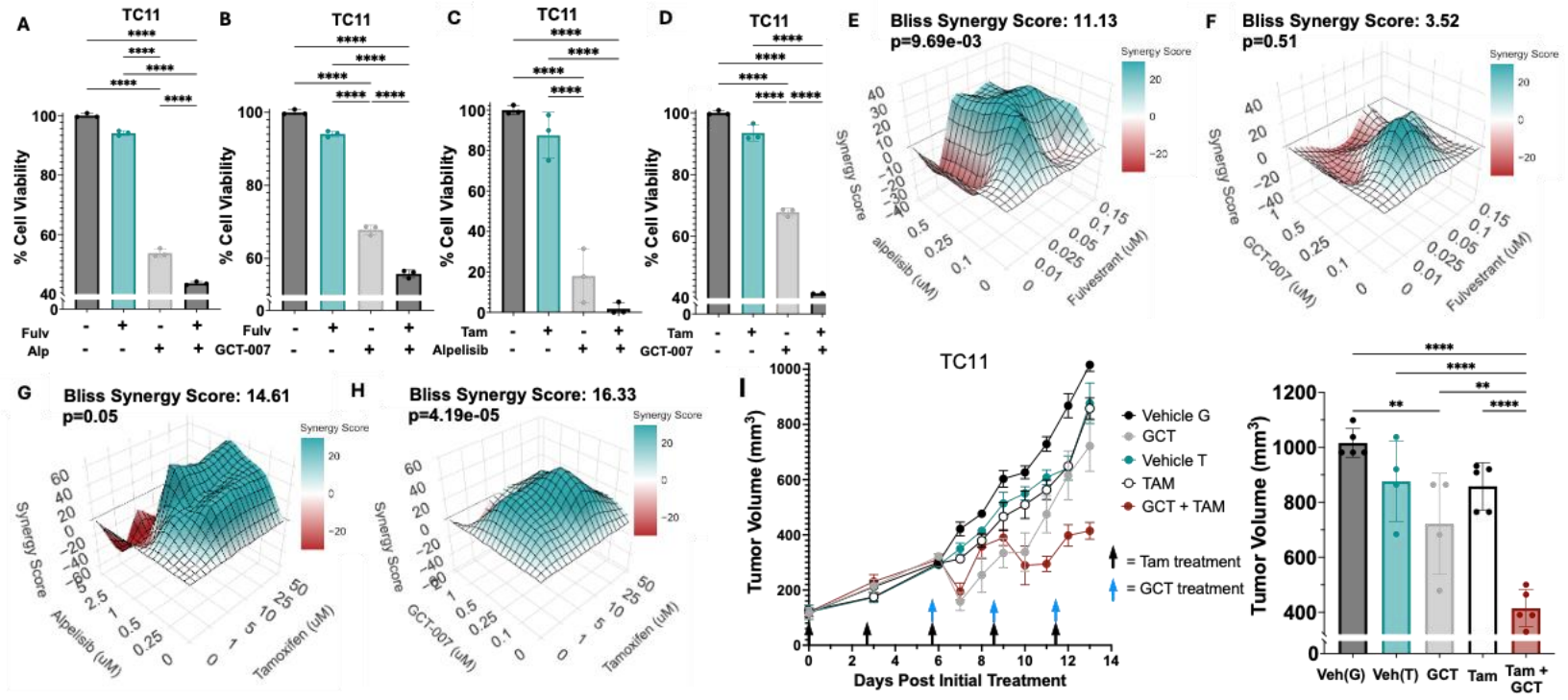

Figure 4. SEMA7A+ tumor growth is inhibited by combination treatment with endocrine therapy and PI3K inhibitors.

Figure 4. SEMA7A+ tumor growth is inhibited by combination treatment with endocrine therapy and PI3K inhibitors.

A) Percent cell viability quantified via crystal violet staining after 48-hour treatment of TC11 cells with DMSO, 8nM fulvestrant, 1μM alpelisib, or the combination, normalized to control. Ordinary one-way ANOVA with Tukey's multiple comparisons test.

B) Percent cell viability quantified via crystal violet staining after 48-hour treatment of TC11 cells with DMSO, 8nM fulvestrant, 0.3μM GCT-007, or the combination, normalized to control. Ordinary one-way ANOVA with Tukey's multiple comparisons test.

C) Percent cell viability quantified via crystal violet staining after 48-hour treatment of TC11 cells with DMSO, 5 μM 4-hydroxytamoxifen, 1μM alpelisib, or the combination, normalized to control. Ordinary one-way ANOVA with Tukey's multiple comparisons test.

D) Percent cell viability quantified via crystal violet staining after 48-hour treatment of TC11 cells with DMSO, 5 μM 4-hydroxytamoxifen, 0.3 μM GCT-007, or the combination, normalized to control. Ordinary one-way ANOVA with Tukey's multiple comparisons test.

E) Bliss synergy score for fulvestrant and alpelisib in TC11 cells.

F) Bliss synergy score for fulvestrant and GCT-007 in TC11 cells.

G) Bliss synergy score for (4-hydroxy)tamoxifen and alpelisib in TC11 cells.

H) Bliss synergy score for (4-hydroxy)tamoxifen and GCT-007 in TC11 cells.

I) Average TC11 tumor volume over time in FVB/N mice, in groups treated with Vehicle, GCT-007, tamoxifen, or the combination. GCT = GCT-007, TAM = tamoxifen. Bar graph: tumor volume at the study endpoint (Day 13). Ordinary one-way ANOVA with Tukey's multiple comparisons test.

Error bars are mean +/- SD (A-D), or mean +/- SEM (I). *$p<0.05$, **$p<0.01$, ***$p<0.001$, ****$p<0.0001$.

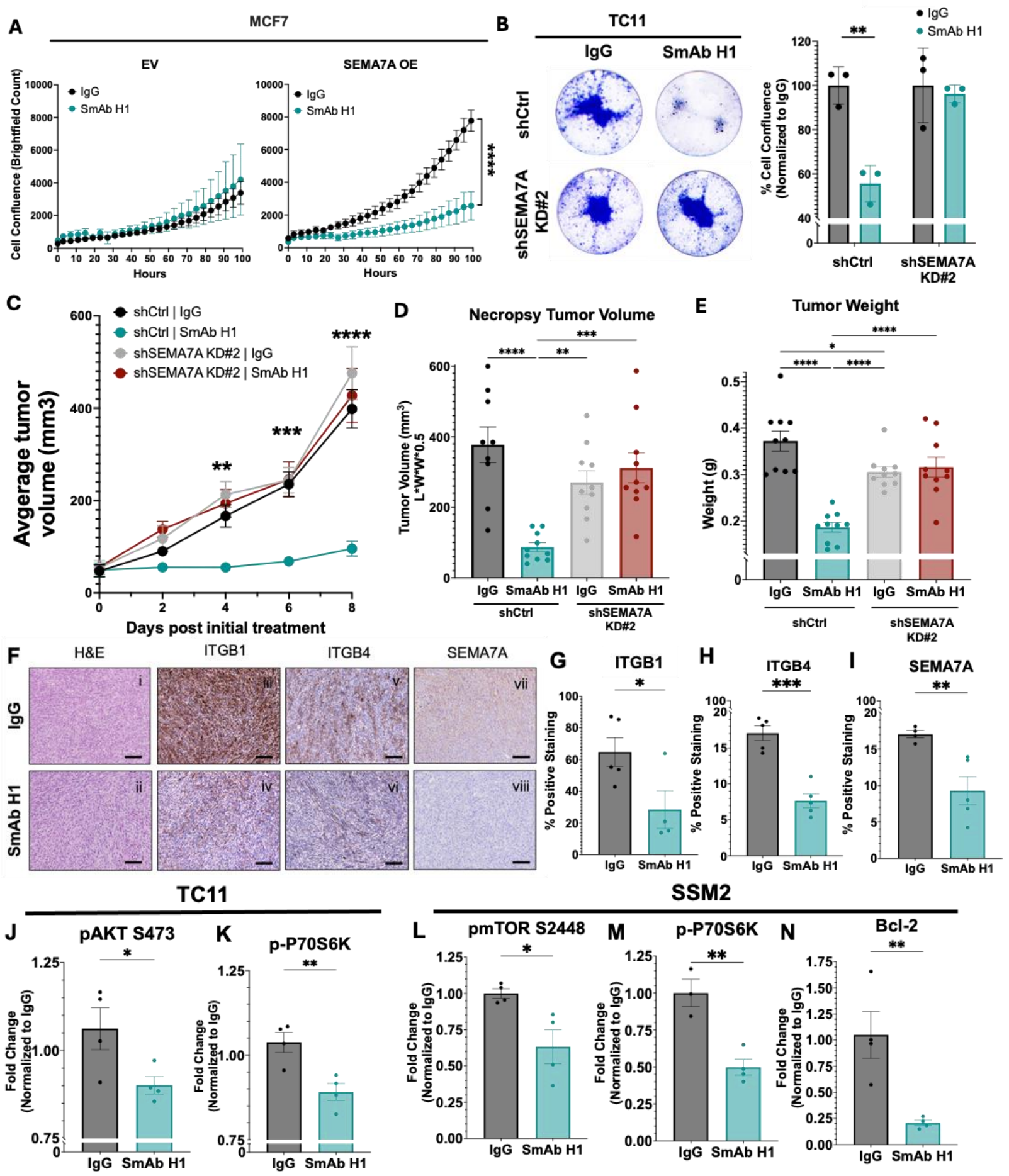

Figure 5. Direct inhibition of SEMA7A using a monoclonal antibody (SmAb H1) effectively reduces tumor growth and AKT signaling in ER+ BC.

Figure 5. Direct inhibition of SEMA7A using a monoclonal antibody (SmAb H1) effectively reduces tumor growth and AKT signaling in ER+ BC.

A) Brightfield cell count measured by BioSpa Live Imaging over 96 hours of MCF7 EV and SEMA7A OE cells treated with mouse IgG1 or 1 μM SmAb H1. Two-tailed unpaired t-test at time = 96 hours.

B) Representative crystal violet staining of TC11 shCtrl and shSEMA7A KD#2 cells after treatment for 48 hours with mouse IgG1 or 1 μM SmAb H1. Bar graph: quantification of all replicates. Ordinary one-way ANOVA with Tukey's multiple comparisons test.

C) Average tumor volume in TC11 tumor-bearing mice over time, with groups receiving IgG1 or SmAb H1 (n=5 per group). Two-tailed unpaired t-test at day 4, 6, and 8 between (shCtrl) IgG and (shCtrl) SmAb H1 groups..

D) Tumor volume calculated using necropsy tumor photos in TC11 shCtrl and shSEMA7A-tumor bearing mice over time with groups receiving IgG1 or SmAb H1 (n=10 per group). Ordinary one-way ANOVA with Tukey's multiple comparisons test.

E) Weight of the tumor (and attached mammary gland) at study endpoint (n=10/group). Ordinary one-way ANOVA with Tukey's multiple comparisons test.

F) Immunohistochemistry staining of ex vivo TC11 tumors from IgG-treated and SmAb H1-treated groups. Scale bars = 50μm. Hematoxylin and eosin (H&E) staining (i-ii), active integrin B1 (9EG7) staining; brown (iii-iv), integrin B4 staining; brown (v-vi), and SEMA7A staining; brown (vii-viii).

G) Quantification of 9EG7 (active ITGB1) IHC staining from all tumors (n=5 per group); Percent positive out of tumor area. Two-tailed unpaired t-test.

H) Quantification of ITGB4 IHC staining from all tumors (n=5 per group); Percent positive out of tumor area. Two-tailed unpaired t-test.

I) Quantification of SEMA7A IHC staining from all tumors (n=5 per group); percent positive out of tumor area. Two-tailed unpaired t-test.

J) Phospho-AKT (S473) protein expression in TC11 SmAb H1-treated tumor lysates compared to control-treated, from RPPA-2 data. Two-tailed unpaired t-test.

K) Phospho-P70S6K protein expression in TC11 SmAb H1-treated tumor lysates compared to control-treated, from RPPA-2 data. Two-tailed unpaired t-test.

L) Phospho-mTOR (S2448) protein expression in SSM2 SmAb H1-treated tumor lysates compared to control-treated, from RPPA-2 data. Two-tailed unpaired t-test.

M) Phospho-P70S6K protein expression in SSM2 SmAb H1-treated tumor lysates compared to control-treated, from RPPA-2 data. Two-tailed unpaired t-test.

N) Bcl-2 protein expression in SSM2 SmAb H1-treated tumor lysates compared to control-treated, from RPPA-2 data. Two-tailed unpaired t-test.

Error bars are mean +/- SD (A-B), or mean +/- SEM (C-E, G-I). *$p<0.05$, **$p<0.01$, ***$p<0.001$, ****$p<0.0001$.

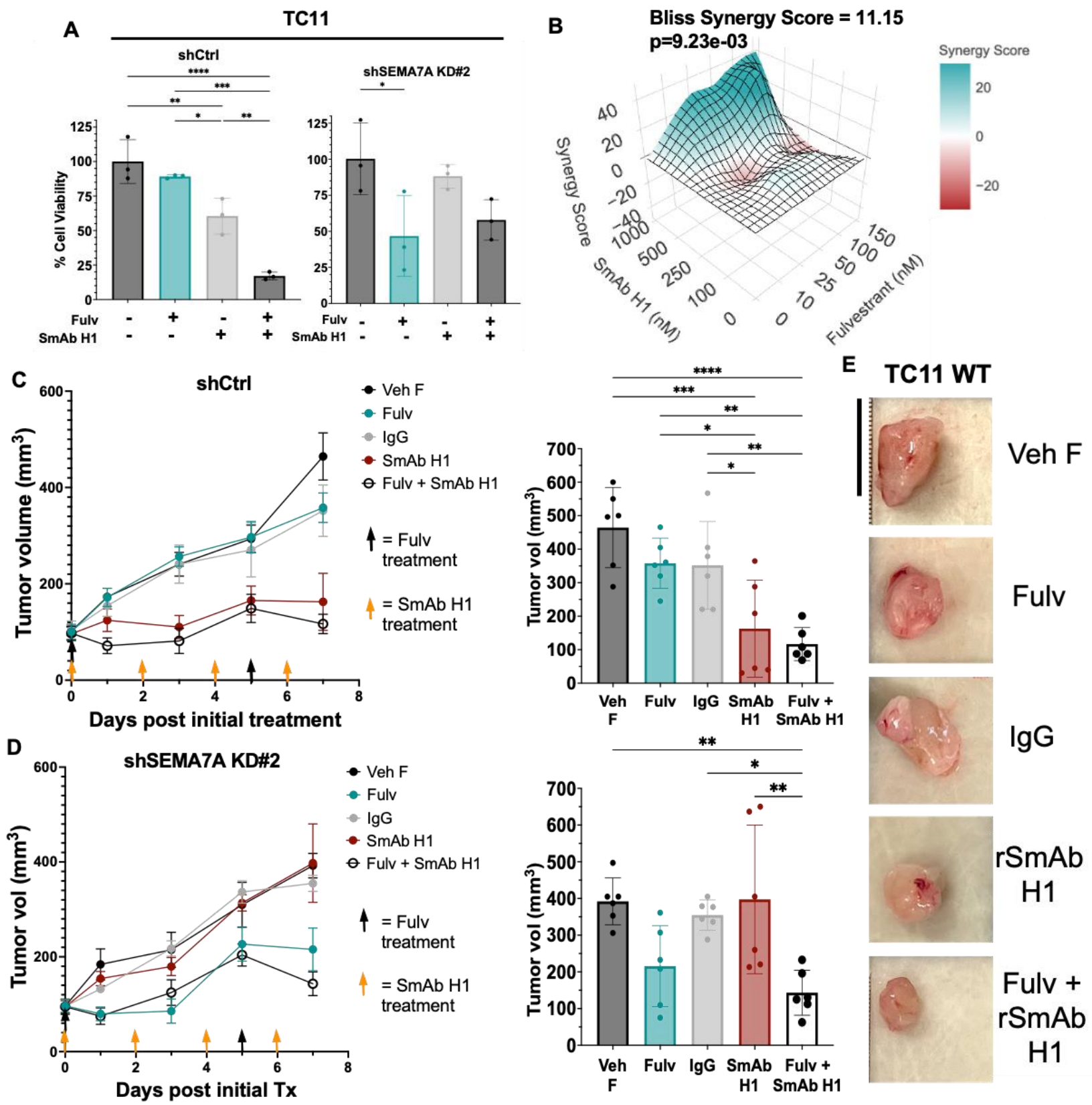

Figure 6. Combination treatment with fulvestrant and SmAb H1 reduces SEMA7A+ ER+ tumor growth.

Figure 6. Combination treatment with fulvestrant and SmAb H1 reduces SEMA7A+ ER+ tumor growth.

A) Cell viability quantified via crystal violet staining after 48-hour treatment of TC11 shCtrl and TC11 shSEMA7A KD#2 cells with DMSO, 8 nM fulvestrant, 1μM SmAb H1, or the combination, normalized to control. Ordinary one-way ANOVA with Tukey's multiple comparisons test.

B) Bliss synergy score for fulvestrant and SmAb H1 in TC11 cells.

C) Average tumor volume in TC11 shCtrl tumor-bearing FVB/N mice over time with groups receiving Vehicle F, IgG1, fulvestrant, SmAb H1 or the combination (n=5 per group). Bar graph: tumor volume at study endpoint (Day 7). Ordinary one-way ANOVA with Tukey's multiple comparisons test.

D) Average tumor volume in TC11 shSEMA7A KD#2 tumor-bearing FVB/N mice over time with groups receiving Vehicle F, IgG1, fulvestrant, SmAb H1 or the combination (n=5 per group). Bar graph: tumor volume at study endpoint (Day 7). Ordinary one-way ANOVA with Tukey's multiple comparisons test.

E) Representative photographs of harvested TC11 tumors treated with Vehicle F, IgG1, fulvestrant, rSmAb H1 or the combination (n=5 per group). Scale bar = 1cm.

Error bars are mean +/- SD (A), or mean +/- SEM (C-D). *$p<0.05$, **$p<0.01$, ***$p<0.001$, ****$p<0.0001$.